Scientific Research Publishing

Journal of High Energy Physics, Gravitation and Cosmology, 2025, 11(3), 1122-1151
https://www.scirp.org/journal/jhepgc
ISSN Online: 2380-4335
ISSN Print: 2380-4327

Behind and Beyond the Standard Model

Rami Rom

Independent Researcher, Zikhron-Ya'akov, Israel
Email: romrami@gmail.com

How to cite this paper: Rom, R. (2025) Behind and Beyond the Standard Model. *Journal of High Energy Physics, Gravitation and Cosmology*, **11**, 1122-1151.
https://doi.org/10.4236/jhepgc.2025.113072

Received: March 28, 2025
Accepted: July 27, 2025
Published: July 30, 2025

Abstract

Similar to Harari's proposal that all leptonic and baryonic matter is composed of four substructure fundamental particles and their antiparticles, $T,V,\tilde{T},\tilde{V}$, we propose that the two light quarks and antiquarks, $u,d,\tilde{u},\tilde{d}$ are the substructure building blocks of matter and also the substructure of the vacuum Pionic fabric. We develop a classical and quantum quark molecular dynamics hybrid scheme to study the Pionic fabric. The Pionic fabric cubic unit cell is assumed to include two pion tetrahedrons having a C_i point group symmetry and may be described by an eight-component spinor. Based on β decay, we propose that electrons are non-elementary, non-point like tetraquarks embedded in the Pionic fabric and together they form electron clouds. A new model for embedded electron tetraquark dynamics is proposed where motion of the embedded electron in the Pionic fabric is performed by a u and d quark exchanges by tunneling through a symmetric double well potential barrier. The rapid quark exchanges transform an embedded electron tetraquark into a pion tetraquark and vice versa in a symmetric reaction that may be seen as a conserved hidden symmetry of the vacuum Pionic fabric. The electron and positron spin states may be related to the underlying quark permutations in one spin state and antiquark permutations in a second spin state. Lattice QCD computations may allow calculating the mass of the embedded electron and pion exotic tetraquarks.

Keywords

The Standard Model (SM), Antimatter, Quantum Vacuum, Exotic Tetraquark

1. Concerns Regarding the Standard Model

1) According to the Standard Model (SM) of particle physics, the building blocks of the universe are quantum fields defined by abstract creation and annihilation operators sums, in contrast to the atomistic point of view where the fundamental building blocks of the universe were particles [1].

2) Paul Dirac thought that better understanding of the vacuum substructure is needed [2] [3]. In contrast to the SM, Dirac thought that electrons are not point like particles and proposed a spherical shell electron model [4].

3) Dirac thought that electrons interact strongly with the vacuum electron-positron virtual pairs and hence are never bare in contrast to the SM path integral approach, where bare electrons propagate in free space in zero-order [5] [6].

4) Harari suggested beyond the SM that all matter (protons, neutrons, electrons and also the interaction bosons, $w^{+/-}$ and Z) are composite particles. Harari named the proposed substructure fundamental particles Rishons, T and V, having an electric charge of a 1/3 and a 0. Accordingly, various combinations of Rishons and their anti-particle pairs $T,V,\tilde{T},\tilde{V}$ create the leptonic and baryonic matter [7].

5) Erwin Schrödinger introduced the idea of a wave packet particle and found that a gaussian wave packet remains coherent with harmonic potential, however in free space, the width of the gaussian wave packet grows rapidly with time [8]. If an electron wave packet is initially localized in a region of an atomic dimension of 10^{-10} meter, the width of the wave packet doubles in about 10^{-16} second and after about a milli-second the wave packet width grows to about a kilometer [9], which is an unreasonable result for a microscopic particle. Is the Schrödinger equation and the path integral approach wrong in free space or maybe the understanding of the vacuum having a fixed potential value is wrong?

2. Addressed Questions

The main questions addressed in the paper are:

1) Does the quantum vacuum have substructure Pionic fabric with a unit cell that may be described by eight-component Spinor?

2) Are the light quarks and antiquarks $u,d,\tilde{d},\tilde{u}$, the fundamental building blocks that comprise all leptonic and baryonic matter?

3) Do the non-elementary, non-point like embedded electron tetraquarks move on the Pionic fabric by rapid u and d and $\tilde{u}$ and $\tilde{d}$ quark permutations?

The Pion tetrahedron and the vacuum substructure are described in Section 3. The classical and quantum quark molecular dynamics hybrid scheme and the Pionic fabric unit cell are described in Section 4. A double well potential model for the electron and pion tetraquarks and the symmetric quark exchange reaction is described in Section 5. The embedded electron and the Pionic fabric cloud are described in Section 6. The positron tetraquarks are described in Section 7. The electron-positron creation and decay embedded in the Pionic fabric are described in Section 8. A proton embedded in the Pionic fabric cell is described in Section 9. The eight-component spinors of the vacuum and the embedded electron and positron dynamics on the Pionic fabric are described in Section 10. A lattice QCD computation of the electron and pion tetraquark mass is proposed in Section 11. Section 12 is a summary.

3. The Pion Tetrahedron and the Vacuum Substructure

We assume that the quantum vacuum is filled with exotic pion tetraquark tetrahedrons that form a Pionic fabric [10]-[14]. We note that the vacuum pion

tetraquark tetrahedrons are not ordinary particles since they are composed of 50% matter and 50% antimatter. We assume that the Pionic fabric quarks and anti-quarks do not annihilate each other, and that their dynamics may be modeled with classical molecular dynamics with additional quark exchange operation described below. We assume that the Pionic fabric unit cell includes two exotic tetraquarks, $u\tilde{d}d\tilde{u}$, each composed of the two light quarks, d and u, and their antiquark pairs, $\tilde{d}$ and $\tilde{u}$ that may be described by eight-component spinor described further in Section 10 below.

A Classical and Quantum Quark Molecular Dynamics Hybrid Scheme

The pion tetraquark molecule is assumed to be composed of a $d\tilde{d}$ and $u\tilde{u}$ mesons having a tetrahedron structure shown in **Figure 1** inside a cubic cell, where the cell size a_π is determined by the classical and quantum hybrid quark molecular dynamics scheme described below. Two pion tetraquark tetrahedron enantiomer molecules may exist obtained by exchanging the positions of two quarks at the tetrahedron vertices that breaks dynamically the chiral symmetry assumed by effective field QCD theory [15]-[21].

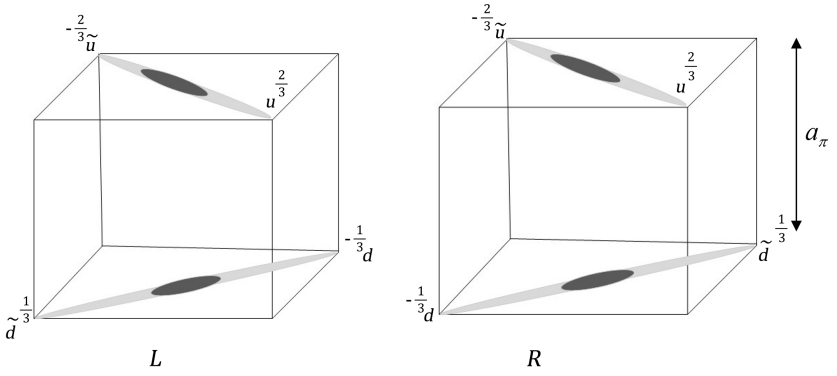

Figure 1. Illustrates the two pion tetraquark tetrahedron enantiomer molecules.

The pion tetraquark Hamiltonian using a quark pair interaction model [22] is:

$$\begin{aligned} H_{\text{pion tetraquark}} = {} & \frac{1}{2}m_u v_u^2 + \frac{1}{2}m_{\tilde{u}} v_{\tilde{u}}^2 + \frac{1}{2}m_d v_d^2 + \frac{1}{2}m_{\tilde{d}} v_d^2 - \frac{4}{9}\frac{e^2}{4\pi\varepsilon_0 r_{u,\tilde{u}}} + \sigma_{u,u} r_{\tilde{u},u} \\ & + \frac{2}{9}\frac{e^2}{4\pi\varepsilon_0 r_{u,\tilde{d}}} + \sigma_{u,d} r\left(u,\tilde{d}\right) - \frac{2}{9}\frac{e^2}{4\pi\varepsilon_0 r_{u,d}} + \sigma_{u,d} r_{u,d} + \frac{2}{9}\frac{e^2}{4\pi\varepsilon_0 r_{\tilde{u},d}} \\ & + \sigma_{u,d} r_{\tilde{u},d} - \frac{2}{9}\frac{e^2}{4\pi\varepsilon_0 r_{\tilde{u},\tilde{d}}} + \sigma_{u,d} r_{\tilde{u},\tilde{d}} - \frac{2}{9}\frac{e^2}{4\pi\varepsilon_0 r_{d,\tilde{d}}} + \sigma_{d,d} r_{d,\tilde{d}} \end{aligned} \quad (1)$$

The classical and quantum quark molecular dynamics hybrid scheme includes in addition to solving Newtonian classical dynamics equations for the four quarks and antiquarks, quark exchange operations that occur by quantum tunneling via a barrier. We assume that an Active Gluonic Center (AGC) is created in the center of hadrons by the quark and antiquark interaction where quark and antiquark pairs exchange positions and velocities of the quark pair according to Equations 2(a)-(b) below. The quark exchanges at the AGC prevent the quarks falling into

the attractive coulomb singularity at short distances $r_{q,\tilde{q}} \sim 0$. The quarks and antiquarks continue their classical periodic trajectories following exactly the path of their pair quark and antiquark after the exchange operation.

$$\boldsymbol{r}_q(t+1) = \boldsymbol{r}_{\tilde{q}}(t),\ \boldsymbol{r}_{\tilde{q}}(t+1) = \boldsymbol{r}_q(t) \tag{2a}$$

$$\boldsymbol{v}_q(t+1) = -\boldsymbol{v}_{\tilde{q}}(t),\ \boldsymbol{v}_{\tilde{q}}(t+1) = -\boldsymbol{v}_q(t) \tag{2b}$$

An example of the pion tetraquark trajectory is shown in Figure 2 for two mesons. The meson quarks and antiquarks, $u\tilde{u}$ and $\tilde{d}d$, are attracted to each other and two quark exchange operations occur at the pion tetraquark AGC, where the classical trajectories of the $\tilde{u}$ (in blue) and u (in orange) occurs simultaneously with the switching of the $\tilde{d}$ (in green) and d quarks trajectories (in red). The exchange operations of the quark and antiquark at the AGC surface occurs instantly and coherently in a single time step and the classical trajectory continues using Newtonian classical dynamics equations.

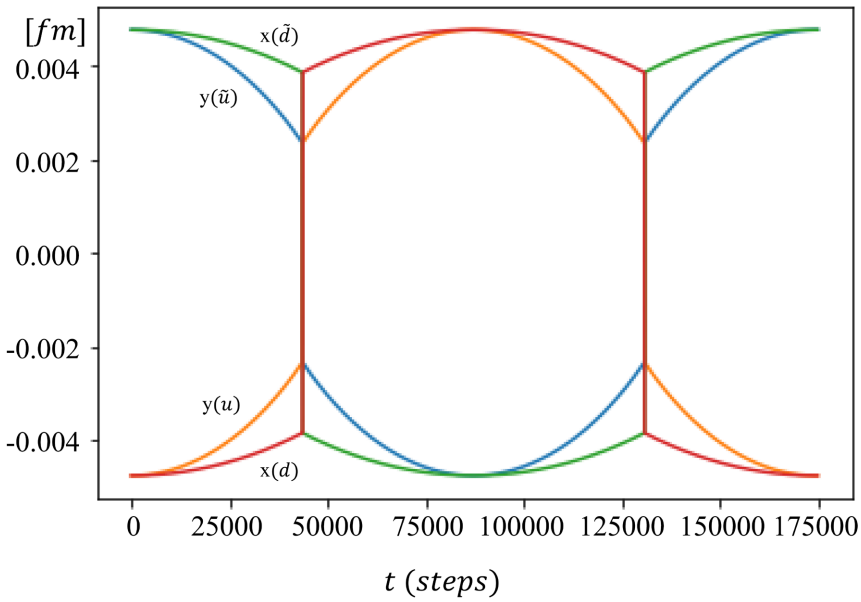

Figure 2. Illustrates the exotic pion tetraquark tetrahedron trajectory with the quark exchange operations at the pion gluonic center (AGC).

4. The Pionic Fabric Cubic Unit Cell Symmetry

A Pionic cubic unit cell that may fill space may include two rotated and flipped pion tetraquark tetrahedrons as shown below. The eight up, down, anti-up and anti-down quarks capture the 8 vertices of the Pionic unit cell where on the 6 faces of the cubic cell there are a chargeless and colorless pions, $\tilde{u}d\tilde{d}u$. We assign the indices below to the first pion tetraquark molecule (1, 2, 3, 4) and the second pion tetraquark molecule (5, 6, 7, 8) (Figure 3).

The Pionic fabric cubic unit cell point group is $C_i(S_2)$, that includes only two symmetry elements, identity and inversion, and two irreducible representations A_g and A_u [22]. The Pionic fabric that may be created extending the Pionic cu-

bic unit cell into a periodic fabric is shown in Figure 4. A d quark (5) has two $\tilde{u}$ and two u quarks surrounding it in the X-Y plane and two $\tilde{d}$ quarks in the Z direction. Similarly, a u quark (2) is surrounded by two $\tilde{d}$ and two d quarks in the X-Y plane and two $\tilde{u}$ quarks in the Z direction. The $\tilde{d}$ and $\tilde{u}$ quarks (3 and 1) have similar quark pair neighbors in the Pionic fabric.

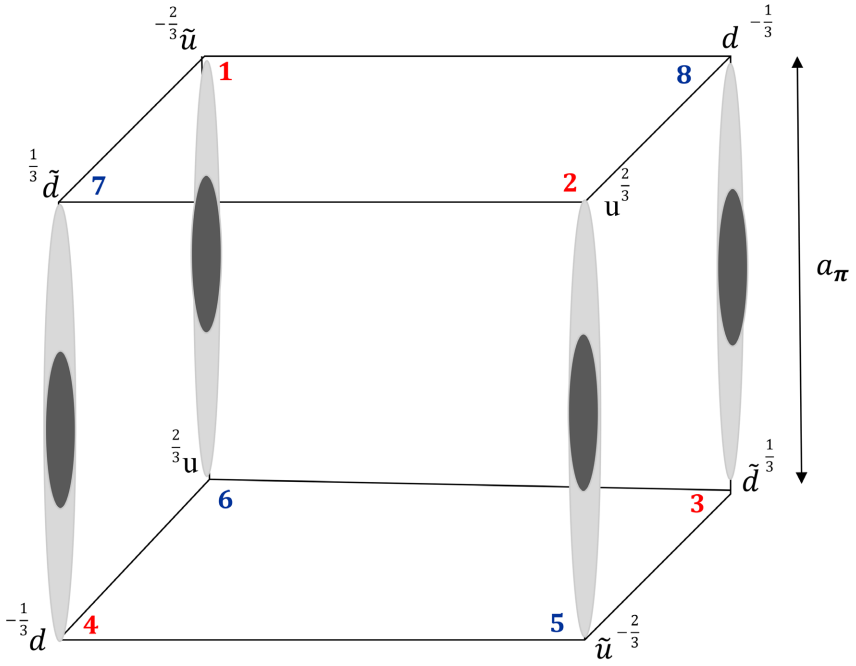

Figure 3. Illustrates Pionic fabric cubic unit cell with C_i point group symmetry.

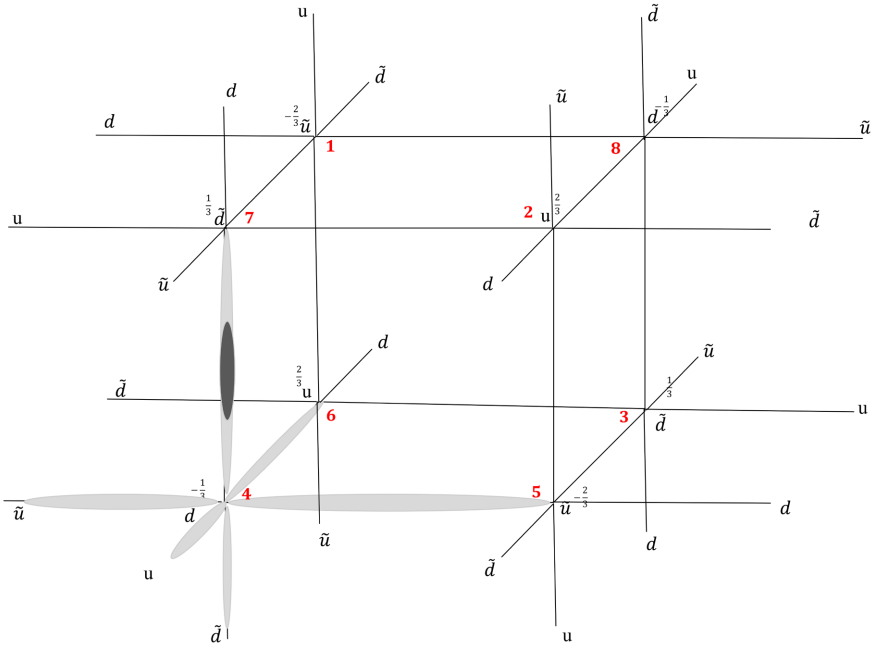

Figure 4. Illustrates the Pionic fabric cubic unit cell and nearest neighbors in the Pionic fabric.

A sum of pair potentials Hamiltonian model for the Pionic unit cell includes pair potentials between all 8 quarks and antiquarks [23] where the sign and magnitude of the Coulomb interaction terms $q_{i.j}$ and the strength of the string tensions $\sigma_{i,j}$ are defined below.

$$H_{\text{pioncell}} = \sum_{i=1}^{8} \frac{1}{2} m_i v_i^2 + \sum_{i,j=1(i<j)}^{8} \left(\frac{q_{i.j} e^2}{4\pi\varepsilon_0 r_{i,j}} + \sigma_{i,j} r_{i,j} \right) \tag{3}$$

$$q_{i.j} = \begin{cases} -\frac{4}{9} & \text{for } \tilde{u}u \text{ pairs} \\ \frac{4}{9} & \text{for } \tilde{u}\tilde{u} \text{ and } uu \text{ pairs} \\ -\frac{2}{9} & \text{for } ud \text{ and } \tilde{u}\tilde{d} \text{ pairs} \\ \frac{2}{9} & \text{for } \tilde{u}d \text{ and } \tilde{d}u \text{ pairs} \\ -\frac{1}{9} & \text{for } d\tilde{d} \text{ pair} \\ \frac{1}{9} & \text{for } dd \text{ and } \tilde{d}\tilde{d} \text{ pairs} \end{cases} \tag{4}$$

$$\sigma_{i,j} = \begin{cases} \sigma_{u,u} & \text{for } \tilde{u}u, \tilde{u}\tilde{u} \text{ and } uu \text{ pairs} \\ \frac{\sigma_{u,u}}{2} & \text{for } \tilde{u}d, \tilde{u}\tilde{d}, \tilde{u}d \text{ and } u\tilde{d} \text{ pairs} \\ \frac{\sigma_{u,u}}{4} & \text{for } \tilde{d}d, \tilde{d}\tilde{d} \text{ and } dd \text{ pairs} \end{cases} \tag{5}$$

Assuming that the Hamiltonian energy vanishes in the ground state, an equation for the cubic cell length a_π as a function of the string tension parameter $\sigma_{u,u}$ is derived.

$$a_\pi = \sqrt{\frac{\frac{10}{9}\left(1-\left(\frac{1}{\sqrt{3}}-1\right)\sqrt{2}\right)\hbar c\alpha}{2\left(\frac{26}{4}+\left(\frac{13}{2}+\frac{5}{2\sqrt{3}}\right)\frac{1}{\sqrt{2}}\right)\sigma_{u,u}}} \tag{6}$$

The quantum vacuum may be filled with infinite number of such zero-energy Pionic unit cells.

Next, the value of the vacuum Pionic cell string tension parameter $\sigma_{u,u} = 1.5\ \text{KeV/fm}$ is determined by the classical and quantum quark molecular dynamics hybrid scheme that generates periodic trajectories shown below in **Figure 5** and **Figure 6**, such that the vibration frequency of the Pionic unit cell quarks and antiquarks is equal to Dirac's electron zitterbewegung frequency $\frac{2m_e c^2}{\hbar}$. The calculated Pionic cell size is $a_\pi = 7.757\times10^{-15}$ meters. Accordingly, the Pionic fabric density in free space is $\rho_{\text{pion fabric}} = \frac{1}{a^3_{\text{pion cell?}}} = 2.1417\times10^{42}\ \frac{\text{pion cells}}{\text{m}^3}$.

The distance between the four $\tilde{u}u$ and $\tilde{d}d$ quark pair of the pion cell are

shown below and illustrate the active gluonic center (AGC) quark exchange operations where the quark exchanges occur vertically between $\tilde{u}(1)$ and $u(6)$, $\tilde{u}(5)$ and $u(2)$, $\tilde{d}(3)$ and $d(8)$, $\tilde{d}(7)$ and $d(4)$ at the cusps (Figure 5).

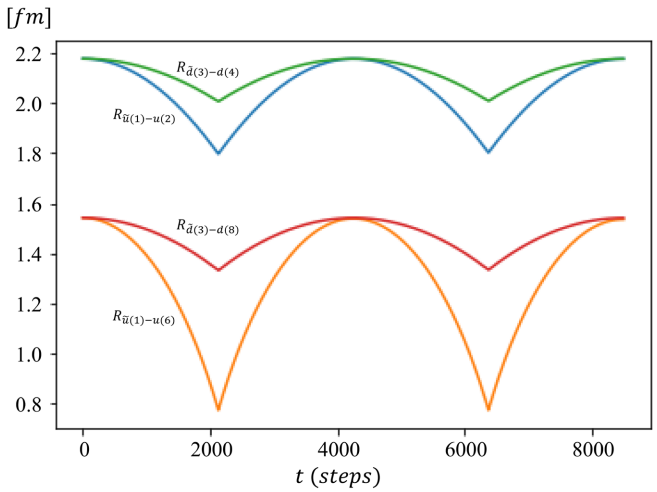

Figure 5. Illustrates the quark and anti-quark pairs distances of the pion cell. The exchange operations occur at the cusps.

The potential and kinetic energies of the Pionic fabric cell quarks and anti-quarks are shown in Figure 6. The Pionic cell vibrates in and out towards the AGC. The quarks kinetic energy grows when the quarks fall in approaching the AGC and then is reduced gradually after the quark exchange occurs at the cusps when the quarks move away from the AGC. We show that the total pion cell energy is zero, since there are infinite number of pion cells in the Pionic fabric, their total energy remains 0. However, the Pionic cells are not static and the quark dynamics are shown by the kinetic and potential energies of the Pionic fabric unit cell in Figure 6 similar harmonic oscillator kinetic and potential energy.

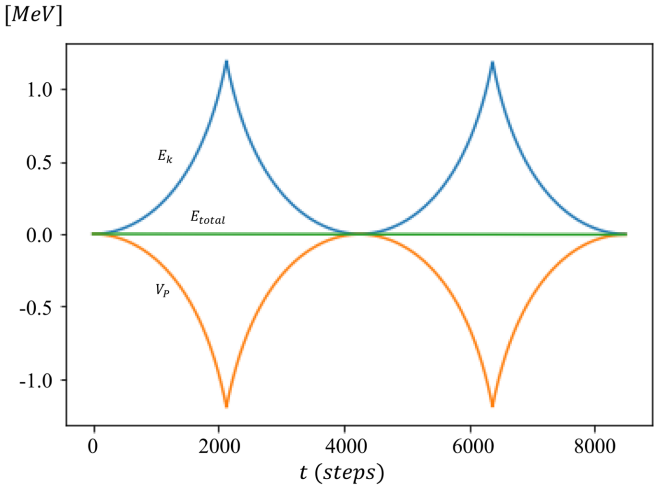

Figure 6. Illustrates the zero-energy Pionic fabric unit cell quarks and antiquarks oscillating potential and kinetic energies.

The X coordinate of the four quarks and anti-quarks of the first pion tetraquark, $\tilde{u}(1)$, $u(2)$, $\tilde{d}(3)$, $d(4)$ are shown below in Figure 7 and the Z coordinate of $\tilde{u}(1)$ and $u(6)$ are shown in Figure 8.

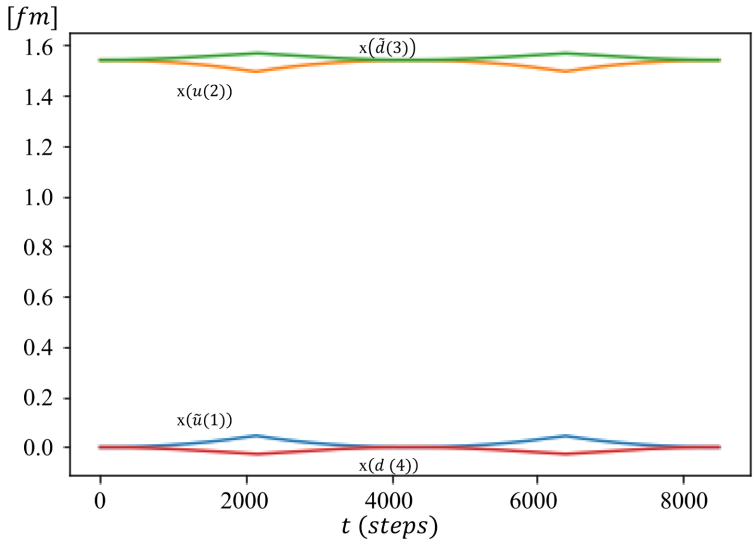

Figure 7. Illustrates the X coordinate of the four quarks and anti-quarks of the first pion tetraquark.

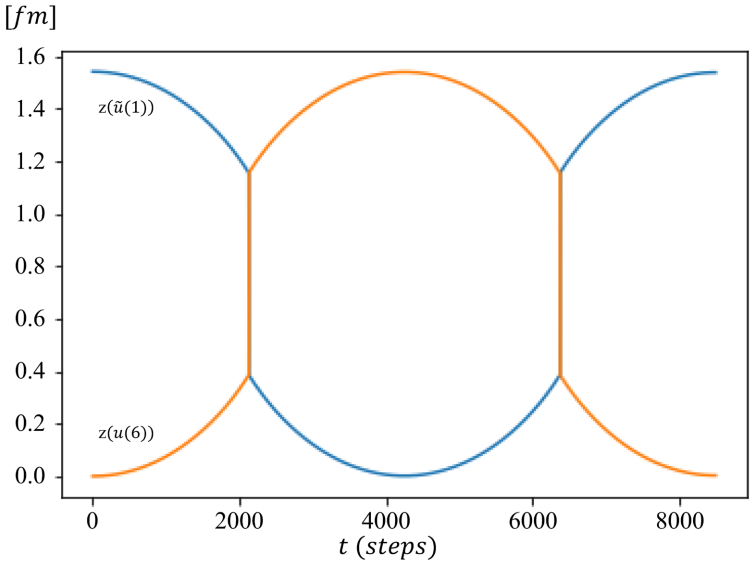

Figure 8. Illustrates the Z coordinate of the $\tilde{u}(1)$ and $u(6)$ quarks.

The Z coordinate of $\tilde{u}(1)$ and $u(6)$ quarks performing the quark exchange at the AGC are shown below. The quark exchanges occur vertically between $\tilde{u}(5)$ and $u(2)$, $\tilde{d}(3)$ and $d(8)$, and $\tilde{d}(7)$ and $d(4)$ (not shown in the figure). We note that the quark molecular dynamics quark exchanges and velocity inversions according to Equations 2(a)-(b) above are equivalent symmetry operations of the Pionic fabric cubic unit cell C_i point group.

5. The Electron and Pion Tetraquarks Double Well

Assuming that the β decay is a second order scattering reaction triggered by the vacuum pion tetraquarks [10], the following β decay reaction generates a proton and a negatively charged exotic tetraquark, $\tilde{u}d\tilde{d}d$ (e^-), that may play the role of an embedded electron mixed with the surrounding pion tetraquarks of the Pionic fabric.

$$udd\left(N\right)+\tilde{u}d\tilde{d}u\left(\pi^{Td}\right)\to udu\left(P^+\right)+\tilde{u}d\tilde{d}d\left(e^-\right) \tag{7}$$

The reaction equation conserves quark number and flavor, and the exotic negatively charged tetraquark, $\tilde{u}d\tilde{d}d$, may be a non-elementary, non-point like embedded electron. A first electron tetraquark state may be $\tilde{u}dd\tilde{d}$, and a second electron tetraquark state may be $\tilde{u}duu$ [10]-[14]. We further note that transforming the electron tetraquark, $\tilde{u}d\tilde{d}d$ (e^-), to a pion tetraquark, $\tilde{u}d\tilde{d}u$ (π^{Td}), may occur by quark exchanges between two adjacent sites in the Pionic fabric. A pion tetraquark tetrahedron may be transformed into an electron tetraquark tetrahedron by a d and a u quark exchanges and vice versa.

After the d and u quark exchanges, for example in vortex 2 of the Pionic fabric unit cell shown in **Figure 3** and **Figure 4**, the energy of the exchanged Pionic unit cell change to the electron rest mass energy of 0.511 MeV due to contracting the Pionic unit cell length a_π by a factor of about 5 to the value $a_\pi = 1.541\times10^{-15}$ meters via setting the string tension parameter to a higher value $\sigma_{u,u} = 38\ \text{KeV/fm}$ comparing to the Pionic cell value $\sigma_{u,u} = 1.5\ \text{KeV/fm}$.

Since the quark exchange reactions are symmetric, e.g. the reactants and products are identical as shown in Equation (9) below, a double well potential model [24] may be used to represent the reaction like in ammonia molecule inversion [25]. Accordingly, the motion of the electron tetraquark tetrahedron in the Pionic fabric is not a free particle motion with a constant potential energy (0 or any non-zero VEV for example) and it occurs via tunneling through a double well potential barrier as shown in **Figure 10** further below. The u and d quarks are exchanged as illustrated in **Figure 9**. Note that the u and d quarks exchanges transfer a unit electric charge from the electron to the pion and vice versa.

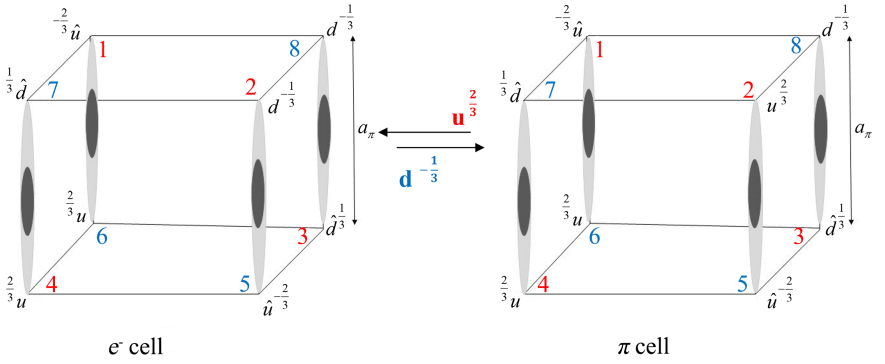

Figure 9. Illustrates an electron tetraquark and a pion tetraquark tetrahedron exchanging quarks (u and d).

The Hidden Internal Symmetry of the Quark Exchange Reactions

The pion and electron quark exchange reaction between Pionic fabric sites *i* and *j* are described in Equation (8) where the *d* and the *u* quarks are exchanged. Since the reactants and products are identical a double well potential model may be used to describe the reaction.

$$\tilde{u}d\tilde{d}d\left(e^{L}\right)_{i}+\tilde{u}d\tilde{d}u\left(\pi^{Td}\right)_{j}\to\tilde{u}d\tilde{d}u\left(\pi^{Td}\right)_{i}+\tilde{u}d\tilde{d}d\left(e^{L}\right)_{j} \tag{8}$$

In the case of the second electron exotic tetraquark state (R), $\tilde{u}$ and $\tilde{d}$ antiquarks may be exchanged according to the following scattering reaction.

$$\tilde{u}d\tilde{d}u\left(\pi^{Td}\right)_{i}+\tilde{u}d\tilde{u}u\left(e^{R}\right)_{j}\to\tilde{u}d\tilde{u}u\left(e^{R}\right)_{i}+\tilde{u}d\tilde{u}u\left(\pi^{Td}\right)_{j} \tag{9}$$

The symmetric d and u and $\tilde{u}$ and $\tilde{d}$ quark exchange reactions between the embedded electron tetraquarks and pion tetraquarks in the Pionic fabric may be seen as a hidden internal symmetry that according to the SM generates a charge and conserved current [1]. The electric charge and current are carried by the *d* and *u* quark exchanges according to Equation (8) and $\tilde{u}$ and $\tilde{d}$ antiquark exchanges according to Equation (9).

A quantum mechanical solution for the double well potential model [24] is presented below and extended further to an electron and pion cloud.

$$\hat{H}=\frac{\hat{P}^{2}}{2m_{e}}+m_{e}\lambda\left(\hat{x}^{2}-a^{2}\right)^{2} \tag{10}$$

m_e is the electron rest mass, $2a$ is the distance between the Pionic fabric sites and the coupling parameter λ may be determined by the potential barrier height, $V_0=m_e\lambda a^4$, where $V_0=\hbar\omega_e=2m_ec^2$. The frequency $\omega_e=\frac{2m_ec^2}{\hbar}$ is Dirac's free space trembling motion zitterbewegung frequency [26] [27].

Figure 10 below illustrates the double well potential for the electron tetraquark tetrahedron and the pion tetraquark tetrahedron quark exchange reaction in adjacent Pionic fabric sites *i* and *j*. With the quantum mechanical double well potential model, the electron motion in the Pionic fabric is via tunneling through the potential barrier. The barrier height $V_0=2m_ec^2$ is assumed to be twice the electron rest mass energy, which is the threshold for electron-positron pair production. Note that the electron tetraquarks on both sides of the double well are identical and hence the electron state ($\tilde{u}d\tilde{d}d$ or $\tilde{u}du\tilde{u}$) is conserved.

The double well symmetric ground state and the antisymmetric first excited state energies and wavefunctions are calculated by diagonalizing the Hamiltonian (Equation (10)) using a Fourier plane wave basis set. The tunneling time, $T_{\text{tunneling}}$, from the left to the right potential well is an inverse function of the energy split between the first anti-symmetric state E_a and the symmetric ground state E_s. With the parameters above, $E_a=1.0463\hbar\omega$ which is just above the potential well barrier and $E_s=0.7004\hbar\omega$ is a bound state inside the potential well. The tunneling time is 5.849×10^{-21} seconds.

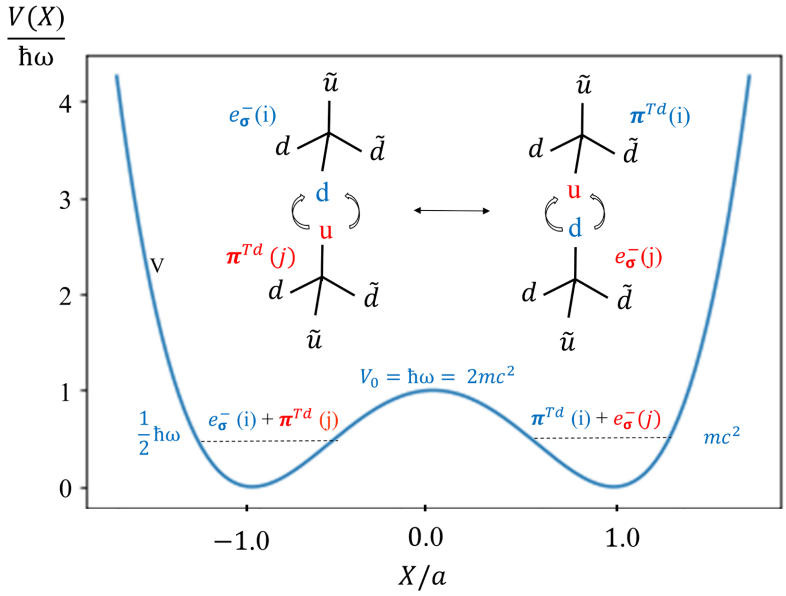

Figure 10. Illustrates the double well potential model for the electron tetraquark tetrahedron and pion tetraquark tetrahedron quark exchange reaction in adjacent sites *i* and *j* in the Pionic fabric.

$$T_{\text{tunneling}} = \frac{\pi\hbar}{E_a - E_s} = 5.849\times10^{-21}\,\text{seconds} \tag{11}$$

A superposition of the symmetric and antisymmetric eigenstates is taken as the initial state $\psi_{t=0}$ describing an electron wave packet located in the left well initially.

$$\psi_0 = \frac{1}{\sqrt{2}}\left(\psi_s + \mathrm{j}\psi_a\right) \tag{12}$$

After half a period the electron wave packet tunnels to the right well

$$\psi_{T_p/2} = \frac{1}{\sqrt{2}}\left(\psi_s \mathrm{e}^{-iE_sT_p/2} + \mathrm{j}\psi_a \mathrm{e}^{-iE_aT_p/2}\right) \tag{13}$$

The electron wave packet continues oscillating between the two wells with a period of $T_p = \frac{2\pi\hbar}{E_a - E_s}$.

The electron velocity in the Pionic fabric may be calculated by dividing the distance between two adjacent wells, $2a$, by the tunneling time.

$$v_e = \frac{2a}{T_{\text{tunneling}}} = \frac{2a\left(E_a - E_s\right)}{\pi\hbar} = 0.44c\left[\frac{\mathrm{m}}{\mathrm{sec}}\right] \tag{14}$$

Note that the electron velocity in this example is 0.44 of the speed of light and that the tunneling frequency is on the time scale of the free space trembling motion zitterbewegung frequency, similar to semi-classical electron models [26] [27].

6. The Embedded Electron and Pionic Fabric Cloud

The double well potential model can be extended to the Pionic fabric where the

electron with the Pionic fabric tetrahedrons are assumed to form a dense and polarized sphere. In the center of the sphere, the double well potential model length may be extremely small below the Compton length. Away from the cloud center, the distance between pion tetraquark tetrahedron cells may increase. After about few Compton lengths, the distance between pion cells may be such that the quark exchange reactions stop. The electron tunneling exponentially decreases and the electron is trapped in the pion cloud sphere by the lack of quark exchange reactions outside the sphere. The electron may be confined by the Pionic fabric sphere that forms the electron cloud.

The following table presents the two lower energy eigenvalues with increasing distance between the two potential wells, $2a$, $4a$ and $6a$ keeping the potential barrier height at the same value, $V_0 = 2m_e c^2$, by changing the value of the coupling parameter λ, $\lambda = \frac{2c^2}{a^4}$, $\lambda = \frac{2c^2}{16a^4}$ and $\lambda = \frac{2c^2}{81a^4}$.

Distance between the two potential wells	$E_a/\hbar\omega$	$E_s/\hbar\omega$	$T_{\text{tunneling}}$ (sec)
$2a$	1.0463	0.7004	5.8495×10^{-21}
$4a$	0.4741	0.4502	8.4577×10^{-20}
$6a$	0.318497	0.31698	1.340×40^{-18}

The electron tunneling time between the two wells is reduced significantly with the growth of the distance between the wells. With the $6a$ distance the tunneling is about 229 times slower than with $2a$ distance (a is defined as the electron Compton length $\frac{\hbar}{m_e c}$). The extremely fast electron wave packet dynamics in the Pionic fabric may be observed in the future with the new attosecond electron microscopy [28].

The Pionic fabric cell length in free space, far from any charged or massive body at ∞ is assumed to be $a_\pi = 7.757 \times 10^{-15}$ meters and after the d quark exchange the u quark charging the pionic cell, the charged pionic cell length contracts by a factor of 5, $a_{\text{pionic cell}}(\text{embeded electron}) = 1.541 \times 10^{-15}$ meters and hence the Pionic density in the electron cloud becomes much higher than in free space,

$$\rho_{\text{pion fabric}}(\text{embeded electron}) = \frac{1}{a^3_{\text{pion cell}}(\text{embeded electron})} = 2.73 \times 10^{44} \frac{\text{pion cells}}{\text{m}^3}.$$

The embedded electron charge polarizes the Pionic fabric in a sphere around the electron since the Pionic fabric cells have built in electric dipole moments and also since the rapid quark exchanges moves the electron from site to site rapidly. We assume that the polarization of the Pionic fabric cloud due to the electron adds a long-range harmonic potential term $\sim \frac{\hbar\omega x^2}{L^2}$, where L is the length scale of the Pionic fabric cloud sphere.

The electron and pion double well potential is extended in one dimension with 10 Pionic fabric sites and with increasing long-range harmonic potential term, 0.25, 1, 2 and $4\frac{\hbar\omega x^2}{L^2}$ for the electron and Pionic cloud model (Figure 11).

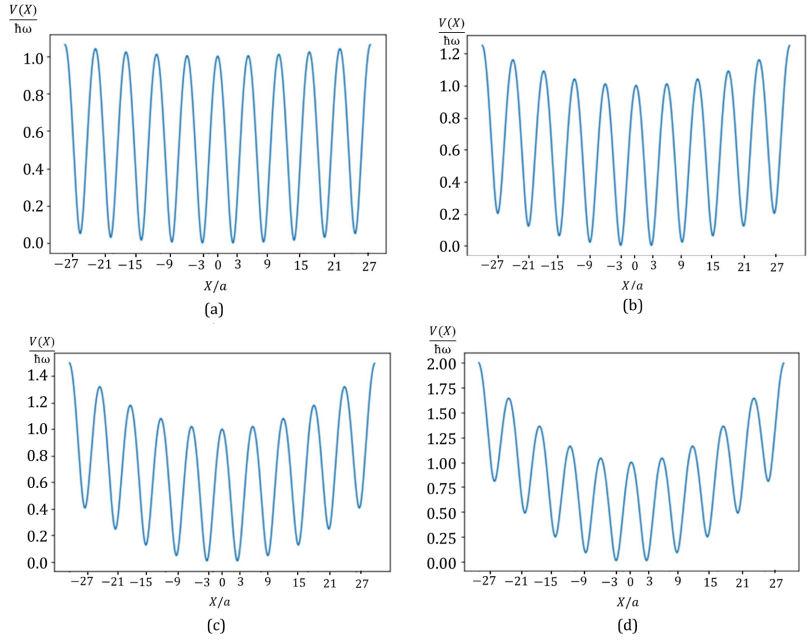

Figure 11. (a)-(d) illustrate the extended electron and Pionic cloud double well potential in one dimension with 10 Pionic fabric sites and increasing long-range harmonic potential term ((a) 0.25, (b) 1, (c) 2 and (d) $4\frac{\hbar\omega x^2}{L^2}$).

The two lowest symmetric, ψ_1, and antisymmetric, ψ_2, eigenfunctions are shown below for the four long-range harmonic potential values. Note that the eigenfunctions peaks are localized in the Pionic fabric wells and that in the two lower states, the tetraquark electron are not localized in a single well, they have finite probability to be found in adjacent wells in the Pionic fabric. With lower long-range harmonic potential term the spread of the initial wave packet is higher (Figure 12).

An initial wave packet can be formed by a superposition of the two lower symmetric and antisymmetric eigenstates, $\psi_0 = \frac{1}{\sqrt{2}}(\psi_1 + \mathrm{j}\psi_2)$. The electron wave packet has high probability to be found in the first few wells on the left initially. After half a period, the wave packet tunnels to the right-hand side wells (in blue). Note that with higher value of the long-range harmonic potential the low eigenstates are localized mainly in a single Pionic fabric site as shown in Figures 13(a)-(d).

The position expectation value of the electron wave packet for 5 time periods for the four long-range harmonic potential values calculated according to Equation (15) are shown in Figures 14(a)-(d).

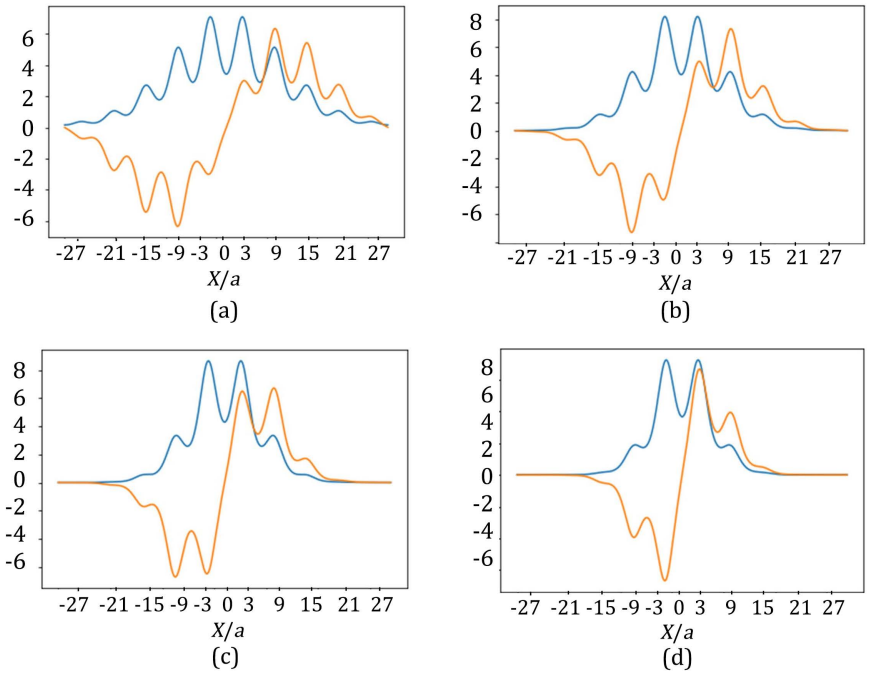

Figure 12. (a)-(d) illustrate the first and second symmetric ψ_1 and antisymmetric ψ_2 eigenfunctions for the four long -range harmonic potential values ((a) 0.25, (b) 1, (c) 2 and (d) $4\frac{\hbar\omega x^2}{L^2}$).

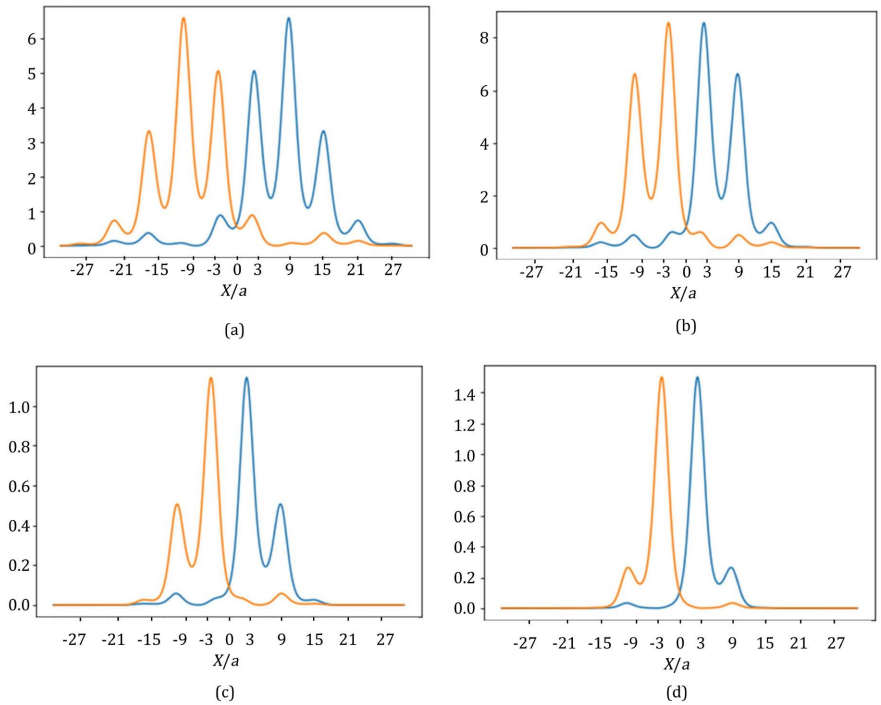

Figure 13. (a)-(d) illustrate the electron wave packet at t = 0 (in orange) and after a half time period (in blue) for the four long -range harmonic potential values ((a) 0.25, (b) 1, (c) 2 and (d) $4\frac{\hbar\omega x^2}{L^2}$).

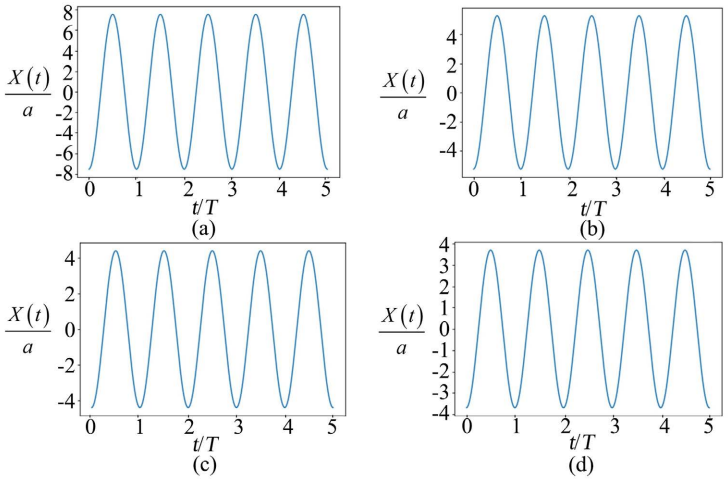

Figure 14. (a)-(d) illustrate the position expectation value of the electron wave packet for 5 time periods for the four long-range harmonic potential values ((a) 0.25, (b) 1, (c) 2 and (d) $4\frac{\hbar\omega x^2}{L^2}$).

$$X(t)=\langle\psi_t|\hat{X}|\psi_t\rangle \tag{15}$$

The position expectation value oscillates between the left-hand side wells to the right-hand side wells. With higher long-range harmonic potential value the oscillation amplitude decreases since the wave packets are more localized in the center.

The higher symmetric ψ_7 and antisymmetric ψ_8 eigenstates are localized in the outer wells. The superposition, $\psi_0=\frac{1}{\sqrt{2}}(\psi_7+\mathrm{j}\psi_8)$, is shown below where the tunneling occurs now between the outer wells (**Figure 15**).

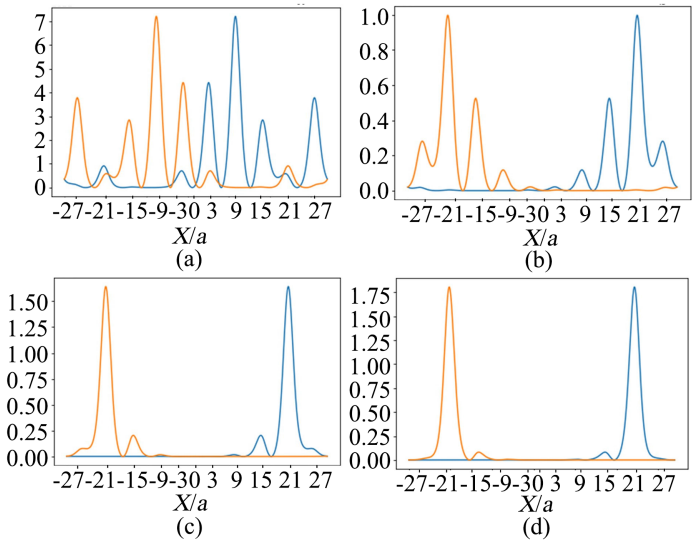

Figure 15. (a)-(d) illustrate the electron wave packet at t = 0 (in orange) and after half time period (in blue) for the four long-range harmonic potential values ((a) 0.25, (b) 1, (c) 2 and (d) $4\frac{\hbar\omega x^2}{L^2}$).

We assume that the polarization effect of the charged electron on the Pionic fabric is to rearrange the Pionic fabric sphere with the speed of light around the electron site. The length parameter a may be changed numerically ($\sim 0.46\frac{\hbar}{m_e c}$ for example) such that the calculated electron velocity according to Equation (14), $v_e = \frac{2a\left(E_a - E_s\right)}{\pi\hbar}$, will be close to the speed of light. In this case, the rearrangement of the Pionic fabric cloud and the tunneling of the electron wave packet occurs at maximal speed and the electron speed is limited to c since the Pionic fabric cannot rearrange faster.

The embedded electron tunnels from site to site in the Pionic fabric extremely fast with the zitterbewegung frequency and it cannot be isolated as a single particle, it is a cloud. Note that the vibration frequency of the quarks of the Pionic fabric is equal to the electron zitterbewegung frequency. The motion of the electron in the Pionic fabric cloud may be in resonance with the Pionic fabric oscillations. Schrödinger suggested that the electron could be described with a wave packet and found that the Gaussian wave packet width grows rapidly with time in free space [8] [9]. The electron wave packet simulations above do not prove the proposed thesis but they show that a confined and coherent embedded electron wave packet can be obtained in a Pionic fabric cloud with underlying quark exchanges via potential barriers. Lattice QCD may allow calculating the mass of the proposed embedded exotic electron and pion tetraquarks. With the embedded electron and Pionic fabric cloud, the embedded electron is never bare. The free particle bare propagator starting point for the perturbative expansion may be the cause for the divergence of the vacuum polarization and electron self-energy Feynman diagram integrals [29]-[31].

7. The Positron Tetraquark Tetrahedron

The positron tetraquark tetrahedrons have a positive charge of the u and $\tilde{d}$ quarks that replace the negative charge of the $\tilde{u}$ and d quarks of the electron tetraquark tetrahedrons as shown below in **Figure 16(a)** and **Figure 16(b)** for the electrons on the left and for the positrons on the right in **Figure 16(c)** and **Figure 16(d)**. Two positron enantiomers, e_R^+ and e_L^+, are equivalent to the two electron enantiomers e_R^- and e_L^-. In the four cases, quark exchanges transform the electrons, or the positrons, to a pion tetraquark tetrahedron (π^{Td}) and vice versa conserving charge and the electron/positron tetraquark state.

8. Electron-Positron Creation and Annihilation in the Pionic Fabric

Electron-positron annihilation in the Pionic fabric may occur by a u and d quark exchanges of an electron tetraquark tetrahedron and a positron tetraquark tetrahedron forming two neutral pion tetraquark tetrahedrons that become part of the Pionic fabric as shown in Equation (16).

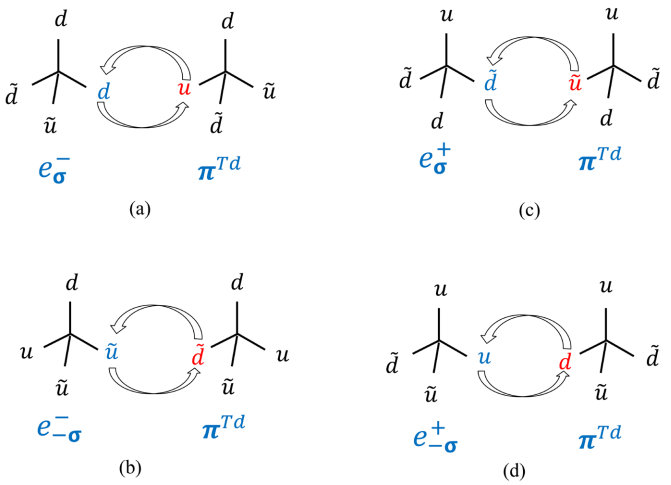

Figure 16. Illustrates electron tetraquark tetrahedron enantiomers (a) and (b) and positron tetraquark tetrahedron enantiomers (c) and (d) exchanging quarks with pion tetraquark tetrahedrons with symmetric reactions such that the electrons and positrons transform to pion tetraquark tetrahedrons and vice versa conserving charge and the electron/positron tetraquark state.

$$\tilde{u}d\tilde{d}d\left(e_L^-\right)+ud\tilde{u}u\left(e_R^+\right)\to\tilde{u}du\tilde{d}\left(\pi^{Td}\right)+\tilde{d}d\tilde{u}u\left(\pi^{Td}\right) \tag{16}$$

An electron tetrahedron in site i in the fabric collides with a positron tetraquark in adjacent site j and the outcome is that both sites after the collision will have neutral pions, where the electron and positron charges and spins are annihilated. The extra energy of the electron and positron may be transferred to the Pionic fabric as electromagnetic excitation wave. Note that in Equation (16) the number and flavor of the quarks are conserved. The quarks are not destroyed nor created in the quark exchanges [10]-[14].

Electron-positron creation may occur in the Pionic fabric cell where a u quark in vortex 4 exchange positions with a d quark in vortex 2 as shown below. The outcome of the quark exchanges is that on the right-hand face of the Pionic cubic cell an electron tetraquark ($\tilde{u}dd\tilde{d}$) is created and on the left-hand face of the Pionic cubic cell a positron tetraquark ($u\tilde{u}u\tilde{d}$) is created. The total charge of the Pionic cubic cell remains 0, however, the electron-positron pair can split and propagate in the Pionic fabric as electromagnetic excitation wave or re-combine by exchanging back the u and d quarks forming back the ground state Pionic fabric unit cell (**Figure 17**).

9. The Proton Embedded in the Pionic Fabric

Protons can be embedded and confined inside the Pionic fabric cell and the quarks of the proton and the Pionic cell have an interesting substructure and correlated dynamics. The existence of the three proton quarks in the Pionic fabric cell contracts the cell length to sub-femtometers. With string tension $\sigma_{u,u}$ of 7.6 GeV/femtometer, the Pionic cell length a_π of the embedded proton is 0.0648×10^{-15} meters such that the embedded proton Pionic cell energy is equal to the rest mass

of the proton of 936.38 MeV. The embedded proton Pionic cell length a_π is shorter by a factor of about 120 comparing to the free space Pionic cell of 7.757×10^{-15} meters calculated with Equations (7)-(10) above (Figure 18).

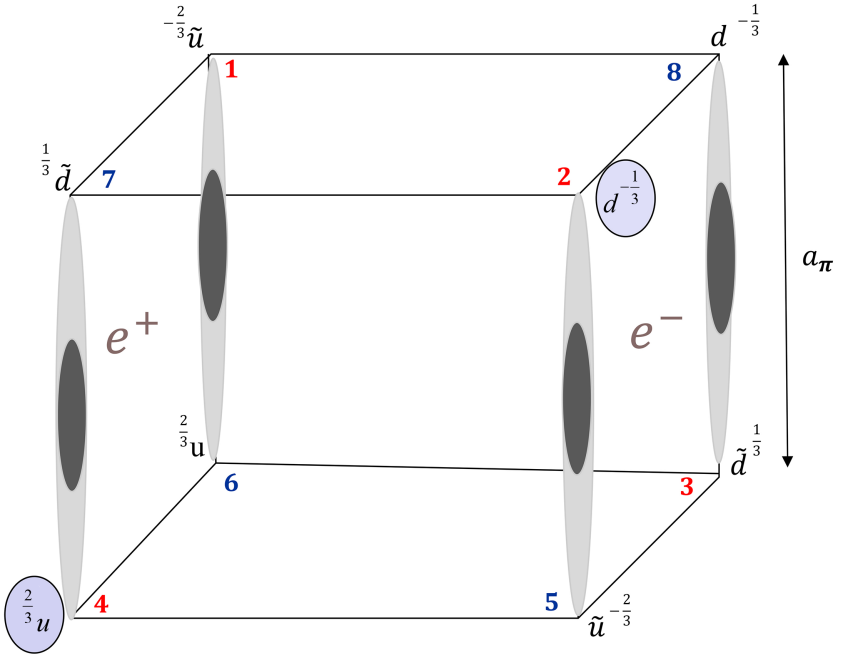

Figure 17. Illustrates the Pionic fabric cubic unit cell with an exchange of a d and a u quark in vertices 2 and 4 that create an electron-positron pair ($u\tilde{u}u\tilde{d}$ (e^+) and $\tilde{u}dd\tilde{d}$ (e^-)) and where the total charge of the cell remains 0.

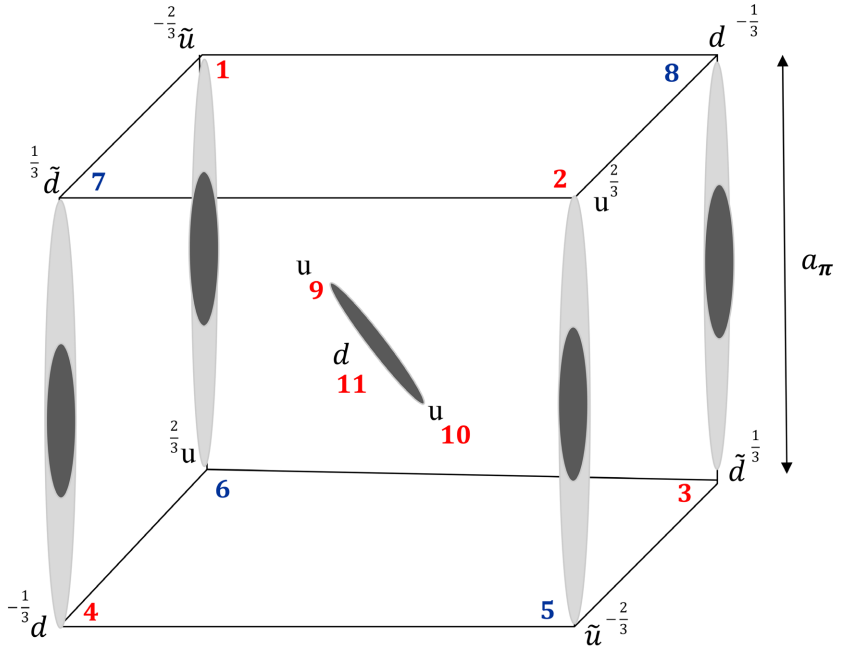

Figure 18. Illustrates the embedded proton in the Pionic cell tilted along the Pionic cell diagonal.

The optimal position of the proton d quark is at the Pionic cell center and the two u quarks are tilted along the cell diagonal towards the two $\tilde{u}$ quarks at the cell corners 1 and 5. The proton two u quarks are attracted to the d quark negative charge and they perform quark position exchanges and velocities flip at the AGC surface at a distance of about 0.76×10^{-18} meters that prevent the u quarks fall into the coulomb singularity at $r_{u,d} \to 0$. The Z coordinate of the pion cell $\tilde{u}_1$ antiquark and u_6 quark and the proton quarks u_9 and u_{10} are shown in the figure below. On the Pionic cell scale, the vibration motion of the quarks is extremely small and almost negligible (Figure 19).

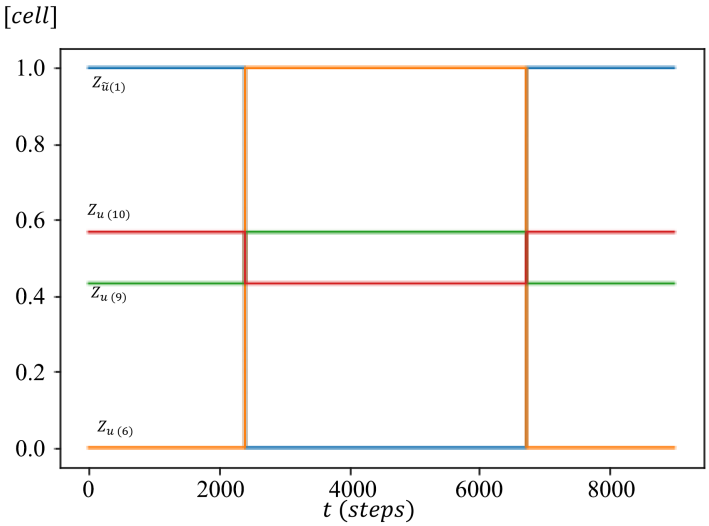

Figure 19. Illustrates the Z coordinate of the pion cell $\tilde{u}_1$ antiquark and u_6 quark and the proton quarks u_9 and u_{10} in the embedded proton pionic cell.

Figure 20 illustrates the energy of the proton and pion cell during two quark exchange operations. Since the Pionic fabric cell symmetry is different than the proton inversion symmetry, the exchange of the Pionic cell quarks and antiquarks, $\tilde{u}_1$ and u_6, $\tilde{u}_5$ and u_2, $\tilde{d}_3$ and d_8, $\tilde{d}_7$ and d_4, and the proton quarks u_9 and u_{10} changes the potential energy of the quarks. The second quark and anti-quark exchange change the potential energy back to the first configuration and hence the energy first grows and then is reduced back as shown below periodically. These energy changes may be seen as energy exchanges between the proton quarks and the Pionic fabric quarks that oscillate around their average static positions.

Figure 21 illustrates the distance between the proton u_9 and u_{10} quarks during the trajectory with two exchange operations at the pion cell AGC. After the first quark exchange operation, the two quarks see different quark configuration of the Pionic fabric cell since each quark is replaced with its antiquark and hence the fall and the bounce back is not fully symmetric. The second bounce at the AGC exchanges back the Pionic fabric cell quarks to their first configuration and then the proton quarks trajectory follows the opposite path and return to their initial position periodically.

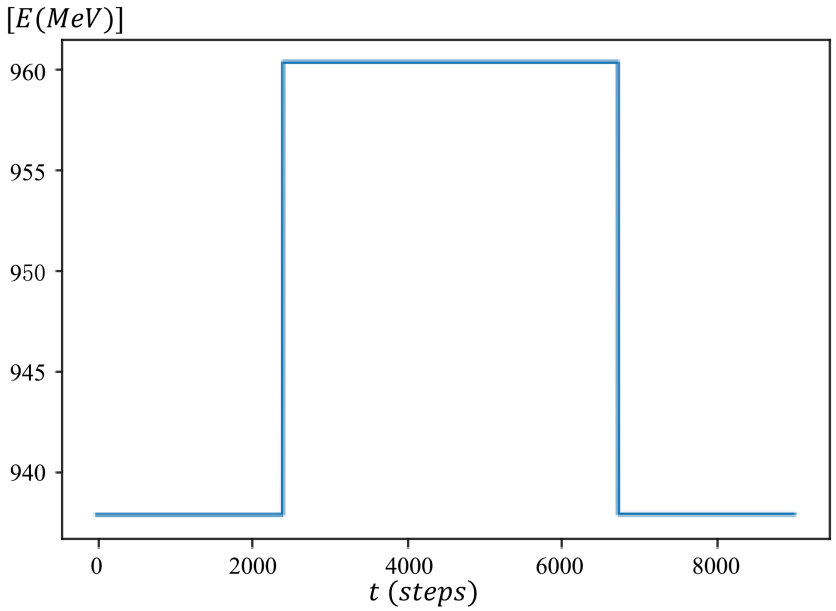

Figure 20. Illustrates the energy of the proton and pion cell during two quark exchange operations.

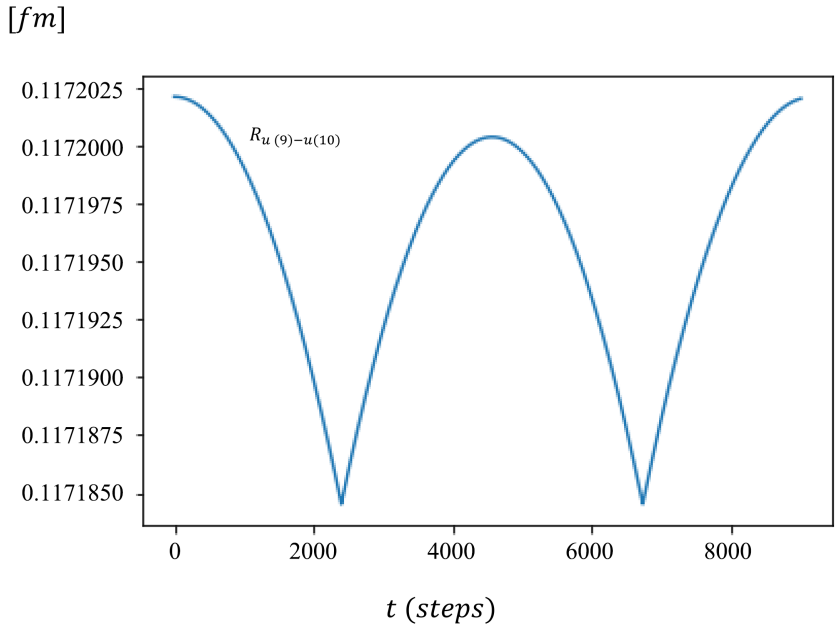

Figure 21. Illustrates the distance between the proton quarks u_9 and u_{10} with the two exchange operations at the cusps.

The Pionic Fabric Density Around Charged and Massive Bodies Model

In the vicinity of massive bodies, the Pionic fabric and Pionic cells may be curved and may have a spherical symmetry where the Pionic cells are forced to reshape and fill a sphere. Near a black hole for example, the Pionic fabric cells may be extremely curved and dense, where far away in space in cosmic voids [32]-[34], the Pionic fabric cells may be diluted and have larger cubic cells in flat space.

In the case of a Hydrogen atom for example, the Pionic fabric density grows from the flat space value of $\rho_{\text{pion fabric}}(\infty)=2.73\times10^{44}\,\frac{\text{pion cells}}{\text{m}^3}$, to a significantly higher density in the vicinity of the embedded proton. The embedded proton pion cell length is 0.0648×10^{-15} meters, two orders of magnitude smaller than the pion cell length in free space of 7.757×10^{-15} meter. We can model the Pionic fabric density in the vicinity of the proton at radius r using the Pionic fabric unit cell length far from the proton in free space and at the proton site using an exponential fall with a parameter λ_p that we will determine next.

$$\rho_{\text{pion fabric}}\left(r-r_p\right)=\frac{1}{a^3_{\text{pion cell}}(\infty)}+\frac{\text{e}^{-(r-r_p)/\lambda_p}}{a^3_{\text{pion cell}}(\text{embeded proton})} \tag{17}$$

Note that in analogy to the exponential fall of the atmospheric density with elevation from earth [10], the Pionic fabric density falls exponentially with distance from the embedded proton and the density gradient will affect the dynamics of particles in the Pionic fabric. For example, the motion of the electron tetrahedron in the fabric via u and d quark exchanges will be sensitive to the fabric density variations since it will change the tunneling rates via the Pionic fabric cells and potential barriers. The electron and Pionic cloud may be confined by the Pionic fabric curvature and density variation due to the embedded proton in the center Pionic cell.

Using the classical and quantum quark molecular dynamics hybrid scheme we calculated the embedded proton Pionic cell length $a_{\text{pionic cell}}(\text{embedded proton})=0.0648\times10^{-15}$, the electron pionic cell length $a_{\text{pionic cell}}(\text{embedded electron})=1.541\times10^{-15}$ meters, and the free space Pionic fabric cell length $a_{\text{pionic cell}}(\infty)=7.757\times10^{-15}$ meters. The Pionic fabric density exponential fall parameter λ_p can be calculated using the three densities' values. Assuming that for the Hydrogen atom at a distance of the Bohr radius, $a_{\text{Bohr}}=0.523\times10^{-10}$ meters, the pionic fabric cell density is:

$$\begin{aligned}&\rho_{\text{pion fabric}}(\text{embedded electron})\\&=\frac{1}{a^3_{\text{pion cell}}(\text{embedded electron})}=2.73\times10^{44}\,\frac{\text{pion cells}}{\text{m}^3}\end{aligned} \tag{18}$$

Next using Equations (17) and (18), we calculate λ_p:

$$\rho_{\text{pion fabric}}\left(a_{\text{Bohr}}\right)=\frac{1}{a^3_{\text{pion cell}}(\infty)}+\frac{\text{e}^{-a_{\text{Bohr}}/\lambda_p}}{a^3_{\text{pioncell}}(\text{proton})}=2.73\times10^{44}\,\frac{\text{pion cells}}{\text{m}^3} \tag{19}$$

$$\lambda_p=\frac{-a_{\text{Bohr}}}{\ln\left(\dfrac{a^{-3}_{\text{pion cell}}(\text{embeded electron})-a^{-3}_{\text{pion cell}}(\infty)}{a^{-3}_{\text{pion cell}}(\text{embeded proton})}\right)}=0.0559\times10^{-10}\,\text{m} \tag{20}$$

λ_p is one order of magnitude smaller than the Bohr radius, however, as shown below, the Pionic fabric density at the Hydrogen atom Bohr radius is about 120 times higher than in free space and it grows exponentially closer to the embedded proton Pionic cell (**Figure 22**).

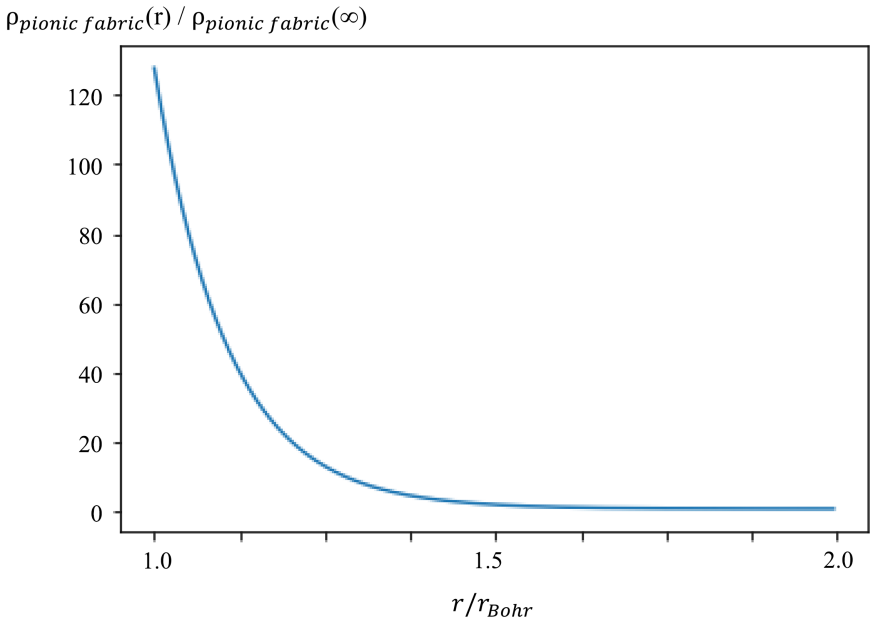

Figure 22. Illustrates the Pionic fabric density as a function of distance from the embedded proton Pionic cell divided by the Pionic fabric density in free space.

In the vicinity of the embedded proton Pionic cell, the Pionic fabric density is extremely high such that the electron motion via quark exchanges between adjacent Pionic cells is inhibited and the electron cannot fall into the coulomb singularity of the proton. On the other limit, far from the embedded proton Pionic cell, the electron motion via tunneling between adjacent Pionic fabric sites is inhibited since the distances between the Pionic fabric cells become too large for the tunneling process. Thus, the density variation of the Pionic fabric induced by the proton confines the embedded electron and Pionic fabric cloud to the atom and prevents the electron fall to the proton.

10. The Eight Component Spinors

A model for the embedded electron and positron dynamics based on the Pionic fabric substructure and eight-component spinors is proposed here. Accordingly, two electron and two positron substructures may be embedded in the Pionic fabric. The first embedded electron type I cell substructure is shown in **Figure 23** below formed by replacing a u quark with a d quark in vortex 2 of a Pionic fabric cell.

The second embedded electron type II cell substructure is shown in **Figure 24** below formed by replacing a $\tilde{d}$ quark with a $\tilde{u}$ quark in vortex 7 of the Pionic fabric cell.

The first embedded positron type I cell structure is shown in **Figure 25** below formed by replacing a $\tilde{u}$ quark with a $\tilde{d}$ quark in vortex 5 of the Pionic fabric cell.

The second embedded positron type II cell structure is shown in **Figure 26** below formed by replacing a d quark with a u quark in vortex 8 of the Pionic fabric cell.

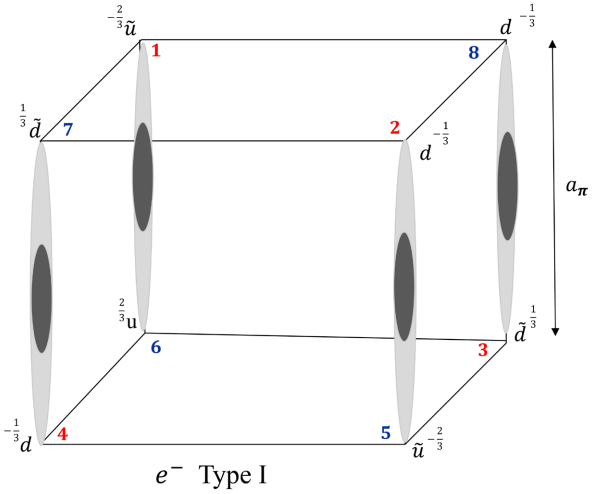

Figure 23. Illustrates embedded electron type I cell.

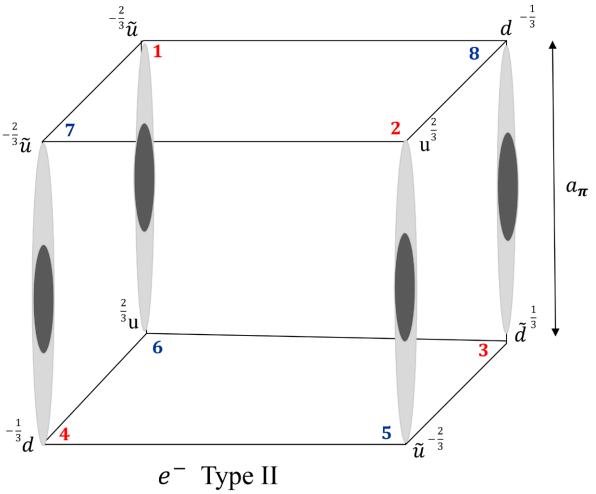

Figure 24. Illustrates embedded electron type II cell.

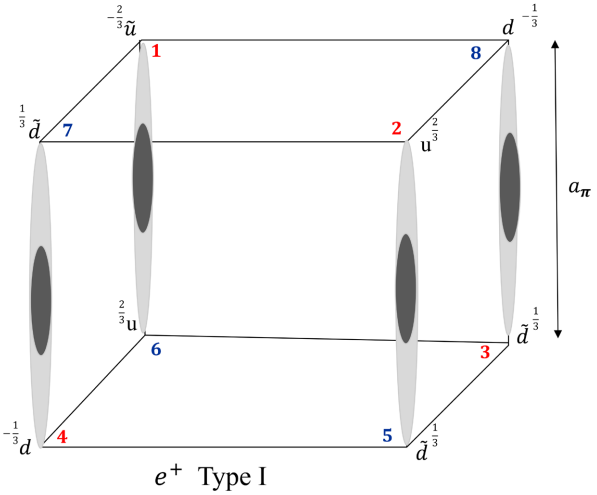

Figure 25. Illustrates embedded positron type I cell.

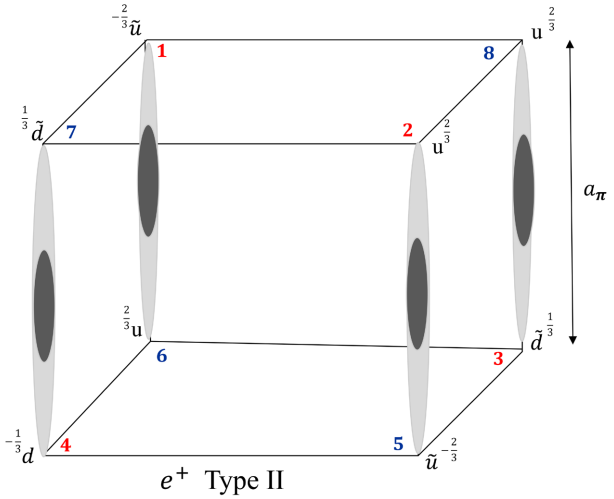

Figure 26. Illustrates embedded positron type II cell.

The Pionic fabric unit cell may be represented by an eight-component spinor and 8*8 identity matrix where the quark ψ_u, ψ_d, $\psi_{\tilde{u}}$ and $\psi_{\tilde{d}}$ are Dirac spinors.

$$\psi_{vacuum} = \begin{bmatrix} 1 & 0 & 0 & 0 & 0 & 0 & 0 & 0 \\ 0 & 1 & 0 & 0 & 0 & 0 & 0 & 0 \\ 0 & 0 & 1 & 0 & 0 & 0 & 0 & 0 \\ 0 & 0 & 0 & 1 & 0 & 0 & 0 & 0 \\ 0 & 0 & 0 & 0 & 1 & 0 & 0 & 0 \\ 0 & 0 & 0 & 0 & 0 & 1 & 0 & 0 \\ 0 & 0 & 0 & 0 & 0 & 0 & 1 & 0 \\ 0 & 0 & 0 & 0 & 0 & 0 & 0 & 1 \end{bmatrix} \begin{bmatrix} \psi_{\tilde{u}} \\ \psi_u \\ \psi_{\tilde{d}} \\ \psi_d \\ \psi_{\tilde{u}} \\ \psi_u \\ \psi_{\tilde{d}} \\ \psi_d \end{bmatrix} \tag{21}$$

The frictionless tunneling motion of the type I embedded electron in the vacuum from a Pionic fabric cell to a neighboring cell that occurs along the long cubic diagonals shown in **Figure 23** can be represented by the following permutation matrix that exchanges for example a d quark in position 2 with a u quark in position 6.

$$\begin{bmatrix} \psi_{\tilde{u}} \\ \psi_u \\ \psi_{\tilde{d}} \\ \psi_d \\ \psi_{\tilde{u}} \\ \psi_d \\ \psi_{\tilde{d}} \\ \psi_d \end{bmatrix} = \begin{bmatrix} 1 & 0 & 0 & 0 & 0 & 0 & 0 & 0 \\ 0 & 0 & 0 & 0 & 0 & 1 & 0 & 0 \\ 0 & 0 & 1 & 0 & 0 & 0 & 0 & 0 \\ 0 & 0 & 0 & 1 & 0 & 0 & 0 & 0 \\ 0 & 0 & 0 & 0 & 1 & 0 & 0 & 0 \\ 0 & 1 & 0 & 0 & 0 & 0 & 0 & 0 \\ 0 & 0 & 0 & 0 & 0 & 0 & 1 & 0 \\ 0 & 0 & 0 & 0 & 0 & 0 & 0 & 1 \end{bmatrix} \begin{bmatrix} \psi_{\tilde{u}} \\ \psi_d \\ \psi_{\tilde{d}} \\ \psi_d \\ \psi_{\tilde{u}} \\ \psi_u \\ \psi_{\tilde{d}} \\ \psi_d \end{bmatrix} \tag{22}$$

Similarly, the motion of the type II embedded electron shown in **Figure 24** on the Pionic fabric can be represented by the next permutation matrix that exchanges a $\tilde{u}$ quark in position 7 with a $\tilde{d}$ quark in position 3.

$$\begin{bmatrix} \psi_{\tilde{d}} \\ \psi_{u} \\ \psi_{\tilde{d}} \\ \psi_{d} \\ \psi_{\tilde{u}} \\ \psi_{u} \\ \psi_{\tilde{d}} \\ \psi_{d} \end{bmatrix} = \begin{bmatrix} 1 & 0 & 0 & 0 & 0 & 0 & 0 & 0 \\ 0 & 1 & 0 & 0 & 0 & 0 & 0 & 0 \\ 0 & 0 & 0 & 0 & 0 & 0 & 1 & 0 \\ 0 & 0 & 0 & 1 & 0 & 0 & 0 & 0 \\ 0 & 0 & 0 & 0 & 1 & 0 & 0 & 0 \\ 0 & 0 & 0 & 0 & 0 & 1 & 0 & 0 \\ 0 & 0 & 1 & 0 & 0 & 0 & 0 & 0 \\ 0 & 0 & 0 & 0 & 0 & 0 & 0 & 1 \end{bmatrix} \begin{bmatrix} \psi_{\tilde{u}} \\ \psi_{u} \\ \psi_{\tilde{d}} \\ \psi_{d} \\ \psi_{\tilde{d}} \\ \psi_{u} \\ \psi_{\tilde{d}} \\ \psi_{d} \end{bmatrix} \tag{23}$$

The electron and positron spin states may be related to the underlying quark permutations in the first spin state and antiquark permutations in the second spin state. Accordingly, the embedded electron and positron dynamics in the Pionic fabric occurs with rapid quark exchanges with adjacent Pionic fabric cells where charge is transferred from the charged embedded Pionic cells to an adjacent neutral Pionic fabric cell by quark exchanges via tunneling as described in Equations (8) and (9) above and represented by the 8*8 permutation matrices and eight-component spinors of Equations (21) and (22). Accordingly, the electron or positron motion occurs by two different mobile particles, a quark exchange dynamic (d and u exchanges) or an antiquark exchange dynamic ($\tilde{d}$ and $\tilde{u}$ exchanges). Note that the two motions can occur independently in the Pionic fabric without collisions and hence the two electron types can share the same electron cloud forming for example an electron pair in an atom or molecule according to Pauli principal. Since an electron pair with opposite spins in the same atomic orbital creates chemical bond, we assume that the dynamic exchange of both quarks and antiquarks in the Pionic fabric cloud stabilizes the shared electron cloud and is favorable energetically compared to a single embedded electron cloud with the d and u exchanges or the $\tilde{d}$ and $\tilde{u}$ exchanges only. In the case of embedded electron-positron collision and annihilation in the Pionic fabric described in Equation (16) above, the double quark exchange reaction will annihilate both charges and will generate a neutral Pionic fabric cell. The complete electronic cloud that included probably millions of contracted Pionic fabric cells will almost instantly expand its volume from the contracted charged Pionic fabric cell length of about 1.541×10^{-15} meters to the value of a Pionic fabric cell in the vacuum of about 7.757×10^{-15} meters. The instant expansion of the Pionic fabric by a factor of about 125 in volume for millions of Pionic fabric cells will generate a significant disturbance in the Pionic fabric that may be seen as the expected two 0.511 MeV electromagnetic waves excitations propagating in the vacuum. Note that in the proposed embedded electron tetraquark dynamics model, the electron-positron charge annihilation in the Pionic fabric does not annihilate the quarks and antiquarks. The quarks and antiquarks are not destroyed nor created, they switch neighbors and remain part of the Pionic fabric.

Coherent Electron Wave Packet Dynamics on the Pionic Fabric

The width of a free electron gaussian wave packet increases with time rapidly in contrast to a coherent state of a particle in a harmonic potential [35]. The dis-

persion of the free particle wave packet will be the same if the Schrödinger equation will be solved with a non-zero fixed potential value. Hence, the SM spontaneous symmetry breaking and the fixed non-zero vacuum expectation value (VEV) of the Higgs mechanism, will not solve the dispersion problem of the free electron wave packet [36]. The behavior of the electron wave packet in a lattice was found to be drastically different if the amplitude and the phase varies on the scale of the lattice constant [37]. The properties of Bloch electrons in solids may be measured by the Quantum Geometric Tensor (QGT) using photoemission spectroscopy [38].

For the embedded electron tetraquark dynamics in the Pionic fabric cloud, we assumed that the electron wave packet is not a gaussian wave packet initially but a superposition of the ground and first excited states in an extended double well potential model, and that it remains a coherent wave packet at later times with no dispersion. The proposed model describes the Pionic fabric and the rapid u and d quark exchange reaction between electrons and pion tetraquarks in adjacent pion fabric cells via double well potential barriers. The symmetric quark exchange reactions may be seen as a conserved hidden symmetry of the Pionic fabric [1]. The quantum vacuum may be described by eight-component spinor extended in the fabric as Bloch spinors.

11. Lattice QCD and the Pionic Fabric

Lattice QCD is a non-perturbative computation scheme for the strong force [39]. Perlovsek *et al.* [40] wrote that the only hadron states found so far are two quark mesons and three quark baryons and that no exotic tetraquark, pentaquark, hybrid meson-gluon or molecular meson states have been confirmed beyond doubt yet. However, there are several candidates in the light tetraquarks and hidden charm sectors, and Perlovsek studied with lattice QCD light tetraquarks that may be the experimentally observed σ and κ mesons.

The quark exchange reactions may be seen as hadron scattering reactions. The d and u quarks for example are exchanged between an electron and pion tetraquarks and the scattering reaction is symmetric since the products are the same as the reactants. Equations (9) and (10) above describe tetraquarks scattering reactions where the electron tetraquark is transformed to a pion tetraquark and vice versa. The tetraquark scattering reactions of Equations (7), (9), (10) and (17) may be studied with lattice QCD [39]-[44] and may allow calculating the mass of the proposed embedded electron the pion tetraquark. We note that the point group symmetry of the Pionic fabric cubic unit cell, $C_i\left(S_2\right)$, includes only two irreducible representations, A_g and A_u [22], that may reduce the complexity of the lattice QCD operators computations.

12. Summary

We assume that the answers to the three questions raised above in Section 2 are positive and consider them as axioms. Accordingly, leptons and hadrons are

quark composed particles. The electron is not the SM point like particle and even not a single particle, it is a cloud of an electron tetraquark and millions of pion tetraquarks part of the Pionic fabric. The Pionic fabric cubic unit cell has a C_i point group symmetry and it includes 50% matter and 50% antimatter and hence the vacuum is not made of ordinary particles as Einstein expected from the gravitational ether [45]. Partanen and Tukkli reformulate QED using eight-component spinors and introduced the generating Lagrangian density of gravity based on the special unitary symmetry of the eight-dimensional spinor space [46] [47]. We propose here that the vacuum and the embedded electrons and positrons may be described by eight-component spinors describing the Pionic fabric cubic unit cell substructure. A new model for embedded electron tetraquark dynamics based on the Pionic fabric substructure is proposed. The rapid quark exchanges transform an embedded electron tetraquark into a pion tetraquark and vice versa in symmetric permutations that may be seen as a hidden internal symmetry [1]. The electron and positron two spin state dynamics may be related to the underlying motion of quark permutations in one spin state and antiquark permutations in the second spin state. The electron and positron chiral states may be related to the structure of the vacuum cubic unit cell. Lattice QCD may allow calculating the mass of the proposed embedded electron and pion tetraquarks.

Conflicts of Interest

The author declares no conflicts of interest regarding the publication of this paper.

References

[1] Quevedo, F. and Schachner, A. (2024) Cambridge Lectures on The Standard Model. arXiv: 2409.09211.https://arxiv.org/abs/2409.09211

[2] Dirac, P. (1928) The Quantum Theory of the Electron. https://www.physics.rutgers.edu/grad/601/QM502_2019/Dirac.pdf

[3] Dirac, P. (1928) Lecture on the Foundation of Quantum Mechanics. https://mediatheque.lindau-nobel.org/recordings/34222/1965-the-foundations-of-quantum-mechanics

[4] Barut, A.O. and Pavsic, M. (1993) Dirac's Shell Model of the Electron and the General Theory of Moving Relativistic Charged Membranes. *Physics Letters B*, **306**, 49-54. https://www.sciencedirect.com/science/article/abs/pii/037026939391136B

[5] Feynman, R. (1963) The Feynman Lectures on Physics, Quantum Mechanics. https://www.feynmanlectures.caltech.edu/III_toc.html

[6] Feynman, R. and Weinberg, S. (1987) The Reason for Antiparticles. https://www.cambridge.org/core/services/aop-cambridge-core/content/view/9D72E7C9045A9C0797DD952678F03C75/9781107590076c1_p1-60_CBO.pdf/the-reason-for-antiparticles.pdf

[7] Harari, H. (1979) A Schematic Model of Quarks and Leptons. *Physics Letters B*, **86**, 83-86. https://doi.org/10.1016/0370-2693(79)90626-9

[8] Kragh, H. (2009) Wave Packet. In: Greenberger, D., Hentschel, K. and Weinert, F., Eds., *Compendium of Quantum Physics*, Springer, 828-830. https://doi.org/10.1007/978-3-540-70626-7_232

[9] Darwin, C.G. (1927) Free Motion in the Wave Mechanics. Proceedings of the Royal Society of London. https://royalsocietypublishing.org/doi/10.1098/rspa.1927.0179

[10] Rom, R. (2023) The Quantum Chromodynamics Gas Density Drop and the General Theory of Relativity Ether. *Journal of High Energy Physics, Gravitation and Cosmology*, **9**, 445-454. https://www.scirp.org/journal/paperinformation.aspx?paperid=124153

[11] Rom, R. (2023) Matter Reactors. *Journal of High Energy Physics, Gravitation and Cosmology*, **9**, 455-460. https://www.scirp.org/journal/paperinformation.aspx?paperid=124154

[12] Rom, R. (2024) Non-Uniform Pion Tetrahedron Aether and Electron Tetrahedron Model. *Journal of High Energy Physics, Gravitation and Cosmology*, **10**, 810-824. https://doi.org/10.4236/jhepgc.2024.102049

[13] Rom, R. (2024) The Pionic Deuterium and the Pion Tetrahedron Vacuum Polarization. *Journal of High Energy Physics, Gravitation and Cosmology*, **10**, 329-345. https://doi.org/10.4236/jhepgc.2024.101024

[14] Rom, R. (2024) QCD's Low Energy Footprint. viXra: 2403.0128. https://vixra.org/abs/2403.0128

[15] Lee, T. (2012) Vacuum Quark Condensate, Chiral Lagrangian, and Bose-Einstein Statistics. *Physics Letters B*, **713**, 270-272. https://doi.org/10.1016/j.physletb.2012.06.014

[16] Brodsky, S.B. and Shrock, R. (2008) On Condensates in Strongly Coupled Gauge Theories. arXiv: 0803.2541. https://arxiv.org/abs/0803.2541

[17] Brodsky, S.B., Roberts, C.D., Shrock, R. and Tandy, P.C. (2010) Essence of the Vacuum Quark Condensate. arXiv: 1005.4610. https://arxiv.org/abs/1005.4610

[18] Buballa, M. and Carignano, S. (2014) Inhomogeneous Chiral Condensates. arXiv: 1406.1367. https://arxiv.org/abs/1406.1367

[19] Byers, N. (1998) E. Noether's Discovery of the Deep Connection Between Symmetries and Conservation Laws. arXiv: physics/9807044. https://arxiv.org/abs/physics/9807044

[20] Burkert, V.D., *et al.* (2022) Precision Studies of QCD in the Low Energy Domain of the EIC. https://www.researchgate.net/publication/365850432_Precision_Studies_of_QCD_in_the_Low_Energy_Domain_of_the_EIC

[21] Paraoanu, G.S. (2014) The Quantum Vacuum. arXiv: 1402.1087. https://arxiv.org/abs/1402.1087

[22] The Ci (S2) Point Group. http://gernot-katzers-spice-pages.com/character_tables/S2.html

[23] Peters, A. (2014) Determination of λ from the Static Quark-Antiquark Potential in Momentum Space. Master's Thesis, Goethe-Universitat Frankfurt am Main. https://itp.uni-frankfurt.de/~mwagner/theses/MA_Peters.pdf

[24] Grabovsky, D. (2021) 115C (QM III): The Double Well. https://web.physics.ucsb.edu/~davidgrabovsky/files-teaching/Double%20Well%20Solutions.pdf

[25] Pengra, D. (2023) The Inversion Spectrum of Ammonia. https://courses.washington.edu/phys432/NH3/ammonia_inversion.pdf

[26] Santos, I.U. (2023) The *Zitterbewegung* Electron Puzzle. *Physics Essays*, **36**, 299-335. https://doi.org/10.4006/0836-1398-36.3.299

[27] Davis, B.S. (2020) Zitterbewegung and the Charge of an Electron. arXiv: 2006.16003.

https://arxiv.org/abs/2006.16003

[28] Hui, D., Alqattan, H., Sennary, M., Golubev, N.V. and Hassan, M.T. (2024) Attosecond Electron Microscopy and Diffraction. *Science Advances*, **10**, eadp5805. https://doi.org/10.1126/sciadv.adp5805

[29] Hooft, G. (2005) Renormalization without Infinities. arXiv: hep-th/0405032v1. https://arxiv.org/pdf/hep-th/0405032

[30] Bergere, M.C. and Zuber, J.Z, (1973) Renormalization of Feynman Amplitudes and Parametric Integral Representation.

[31] Blechman, A.E. (2002) Renormalization: Our Greatly Misunderstood Friend.

[32] Keenan, R.C., Barger, A.J. and Cowie, L.L. (2013) Evidence for a ~300 Megaparsec Scale Under-Density in the Local Galaxy Distribution. *The Astrophysical Journal*, **775**, Article 62. https://doi.org/10.1088/0004-637x/775/1/62

[33] Banik, I. (2023) Do We Live in a Giant Void? It Could Solve the Puzzle of the Universe's Expansion.

[34] Mazurenko, S., Banik, I., Kroupa, P. and Haslbauer, M. (2023) A Simultaneous Solution to the Hubble Tension and Observed Bulk Flow within 250 h^{-1} Mpc. *Monthly Notices of the Royal Astronomical Society*, **527**, 4388-4396. https://doi.org/10.1093/mnras/stad3357

[35] Heller, E.J. (1975) Time-Dependent Approach to Semiclassical Dynamics. *The Journal of Chemical Physics*, **62**, 1544-1555. https://doi.org/10.1063/1.430620

[36] Melo I. (2019) Higgs Potential and Fundamental Physics. arXiv: 1911.08893v1. https://arxiv.org/pdf/1911.08893

[37] Schönhammer, K. (2019) Unusual Broadening of Wave Packets on Lattices. arXiv: 1902.07952. https://arxiv.org/abs/1902.07952

[38] Kang, M., *et al.* (2024) Measurements of the Quantum Geometric Tensor in Solids. arXiv: 2412.17809. https://arxiv.org/abs/2412.17809

[39] Ukawa, A. (2015) Kenneth Wilson and Lattice QCD. arXiv: 1501.04215. https://arxiv.org/abs/1501.04215

[40] Boyle, P., *et al.* (2022) Lattice QCD and the Computational Frontier. arXiv: 2204.00039. https://arxiv.org/abs/2204.00039

[41] Prelovsek, S., *et al.* (2010) Lattice Study of Light Scalar Tetraquarks with I = 0, 2, 1/2, 3/2: Are σ and κ Tetraquarks? arXiv: 1005.0948. https://arxiv.org/abs/1005.0948

[42] Pacheco, E.O., Collins, S., Leskovec, L., Padmanath, M. and Prelovsek, S. (2023) Doubly Charmed Tetraquark: Isospin Channels and Diquark-Antidiquark Interpolators. arXiv: 2312.13441. https://arxiv.org/abs/2312.13441

[43] Alexandrou, C., Berlin, J., Finkenrath, J., Leontiou, T. and Wagner, M. (2019) Tetraquark Interpolating Fields in a Lattice QCD Investigation of the (2317) Meson. arXiv: 1911.08435. https://arxiv.org/abs/1911.08435

[44] Meng, L., Chen, Y., Ma, Y. and Zhu, S. (2023) Tetraquark Bound States in Constituent Quark Models: Benchmark Test Calculations. *Physical Review D*, **108**, Article ID: 114016. https://doi.org/10.1103/physrevd.108.114016

[45] Einstein, A. (1920) Ether and Relativity. https://mathshistory.st-andrews.ac.uk/Extras/Einstein_ether/

[46] Partanen, N. and Tulkki, J. (2024) QED Based on an Eight-Dimensional Spinorial Wave Equation of the Electromagnetic Field and the Emergence of Quantum Gravity. *Physical Review A*, 1**09**, Article 032224. https://doi.org/10.1103/PhysRevA.109.032224

[47] Partanen, N. and Tulkki, J. (2025) Gravity Generated by Four One-Dimensional Unitary Gauge Symmetries and the Standard Model. *Reports on Progress in Physics*, **88**, Article 057802. https://doi.org/10.1088/1361-6633/adc82e